Computational Analysis of an Instantaneous Chemical Reaction in a T-Microreactor

Dieter Bothe
Mathematical Modeling and Analysis, Center of Smart Interfaces, TU Darmstadt, Germany

Alexander Lojewski
Chair for Mathematics, Center for Computational Engineering Science, RWTH Aachen, Germany

Hans-Joachim Warnecke
Chemical Engineering, Faculty of Sciences, University of Paderborn, Germany

DOI 10.1002/aic.12067
Published online October 13, 2009 in Wiley InterScience (www.interscience.wiley.com).

We extend and apply a method for the numerical computation of convective and diffusive mixing in liquid systems with very fast irreversible chemical reaction to the case of unequal diffusivities. This approach circumvents the solution of stiff differential equations and, hence, facilitates the direct numerical simulation of reactive flows with quasi-instantaneous reactions. The method is validated by means of a neutralization reaction which is studied in a T-shaped micromixer and compared with existing experimental LIF-data. Because of their large are-to-volume ratio, microreactors are well suited for fast chemical reactions which are seriously affected by the slow diffusive transport in aqueous media. Numerical computations for different reactor dimensions reveal the fact that, in a dimensionless setting, the obtained conversion is independent of the reactor size, if the flow conditions are the same. This corresponds to an increase of space-time-yield proportional to the square of the inverse scale factor. © 2009 American Institute of Chemical Engineers *AIChE J,* 56: 1406–1415, 2010
Keywords: quasi-instantaneous chemical reaction, neutralization, reaction–convection–diffusion equation, T-shaped microreactor, 3D fully resolved numerical simulations

Introduction

The interplay between transport processes like convection and diffusion with chemical transformations in real world applications is highly complex. Most research work which investigates reactive mixing focuses of turbulent flows.[1,2] Nevertheless, in the fields of highly viscous processing as well as, more recently, microreactor engineering, reactive mixing under complex but laminar flow conditions is an important issue as well.[3–6] Irrespective of the flow conditions, the numerical simulation of reactive mixing in liquids with finite rate chemistry according to

$$\partial_t c_i + \mathbf{u} \cdot \nabla c_i = \frac{1}{ReSc_i} \Delta c_i - \frac{d_h}{L} Da_I c_i^n \qquad (1)$$

in case of a reaction of n-th order, say, is only possible if the Damköhler(I)-number is not too large. Otherwise, the system (1) of differential equations would become extremely stiff. Therefore, the numerical simulation of reactive mixing with very fast chemical reactions requires special solution methods in order to avoid unacceptably small time steps. In the limiting

Correspondence concerning this article should be addressed to Dieter Bothe at bothe@csi.tu-darmstadt.de.

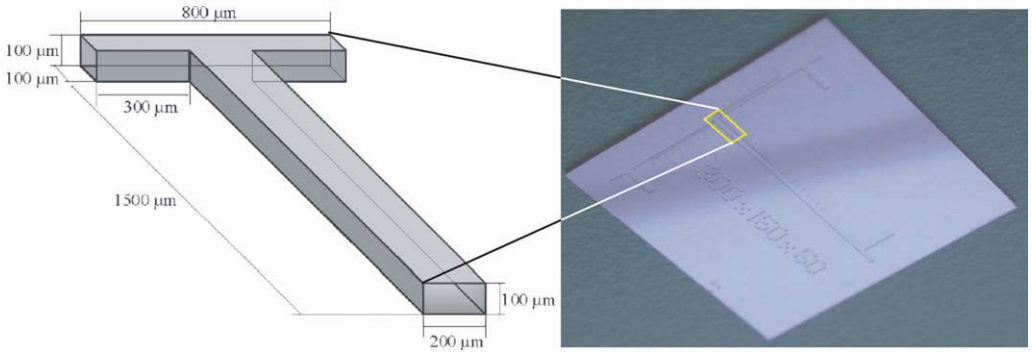

Figure 1. Photograph of a silicon chip with the etched micro channel (left).

The yellow rectangle denotes the computational domain. Physical dimensions of the computational domain (right). [Color figure can be viewed in the online issue, which is available at www.interscience.wiley.com.]

case of quasi-instantaneous chemical reactions, i.e. in situations when the chemical reaction takes place on a time scale which is several orders of magnitude smaller than those of the transport processes, the stiffness of the corresponding system of partial differential equations can often be removed by passage to the limit of infinitely fast (i.e. quasi-instantaneous) chemical reactions. The latter typically yields an excellent approximation in case of, e.g., neutralizations or radical reactions. The basic idea is to remove the source terms which come from the fast reaction by means of an appropriate linear combination of the involved species. This leads to fewer equations, but this loss of information is compensated by the additional fact that reactants which react in an instantaneous reaction cannot coexist on the level of local concentrations. With this approach, the changes in species concentration are finally modeled by solving a scalar transport equation which describes the difference between the molar concentrations of both reactants. This equation does no longer contain the reactive source terms which cause the large stiffness. Because of the fact of non-coexistence of the reactants, the computed scalar field represents both reactants simultaneously. Hence, this approach allows for simulation of reactive mixing in complex flows with very fast chemical reactions. In principle, this approach has already been used in Toor and Chiang[7] for theoretical purposes. Two decades ago it has been employed to study diffusion-limited reactions in lamellar systems with diffusion acting normal to the lamellae.[8–11] In all papers mentioned above the reacting species are assumed to have the same diffusivity which allows reducing the considered reaction-diffusion systems to the diffusion equation which is analytically treatable. Just recently, this approach has also been applied for the simulation of infinitely fast reactions in a 3D open Stokes flow,[12] where again equal diffusivities are assumed. Especially for numerical studies, this rather restrictive assumption is not needed and we do not impose it here.

Since very fast reactions will usually occur as a part of larger systems in which the products undergo consecutive chemical reactions, we include in our approach a way to calculate the local distribution of the generated products. For this purpose the source term describing the fast (instantaneous) chemistry, which still appears within the transport equation of the product, is replaced by the equivalent local net transport of one of the reactants. This extends our previously reported results.[13]

Although the theoretical considerations are independent of a specific reactor type or a certain type of flow, we perform the numerical simulations for a T-microreactor with stationary but complex laminar flow. The considered engulfment flow regime shows good convective mixing in cross sectional directions because of the superimposed secondary flow.[14,15] Because of the well-defined operational conditions in microchannels, such systems allow for experimental validations. The specific type of a T-shaped microreactor is, on one side, a prototype of a simple mixer and on the other side a junction element often involved in more complex micro-systems. Figure 1 displays the investigated T-microreactor. More information on non-reactive mixing in such T-microchannels at various flow regimes can be found, e.g., in Bothe et al.[14,15] and in Dreher et al.[16]

Mathematical Model

Using appropriate boundary conditions, the Navier-Stokes equations provide the velocity field for the convective species transport in an incompressible Newtonian liquid. In non-dimensional form these read as

$$\nabla \cdot \mathbf{u} = 0, \quad \partial_t \mathbf{u} + \mathbf{u} \cdot \nabla \mathbf{u} = -\nabla p + \frac{1}{Re} \Delta \mathbf{u}. \tag{2}$$

The time dependent variations of molar species concentrations of an irreversible chemical reaction of second order,

$$A + B \overset{k \to \infty}{\longrightarrow} P,$$

are described by three reaction–convection–diffusion equations. Each of them represents the balance of species mass and includes a source term representing the chemical reaction. In case of mass action kinetics, the source term is modeled as the product of the molar concentrations of the reacting species, the rate constant and the species specific stoichiometric coefficient. This leads to the system

$$\partial_t c_\mathrm{A} + \mathbf{u} \cdot \nabla c_\mathrm{A} = \frac{1}{Re\, Sc_\mathrm{A}} \Delta c_\mathrm{A} - \frac{d_h}{L} Da_\mathrm{I} c_\mathrm{A} c_\mathrm{B}, \tag{3}$$

$$\partial_t c_\mathrm{B} + \mathbf{u} \cdot \nabla c_\mathrm{B} = \frac{1}{Re\, Sc_\mathrm{B}} \Delta c_\mathrm{B} - \frac{d_h}{L} Da_\mathrm{I} c_\mathrm{A} c_\mathrm{B}, \tag{4}$$

$$\partial_t c_P + \mathbf{u} \cdot \nabla c_P = \frac{1}{Re\, Sc_P} \Delta c_P - \frac{d_h}{L} Da_{\mathrm{I}} c_{\mathrm{A}} c_{\mathrm{B}}. \tag{5}$$

where

$$Re = \frac{U\, d_h}{\nu}, \quad Sc_i = \frac{\nu}{D_i}, \quad Da_{\mathrm{I}} = \frac{k\, Lc^{n-1}}{U} \tag{6}$$

denote the Reynolds, Schmidt and Damköhler number, respectively.

Since the rate constant tends to infinity in the limit of an instantaneous reaction and furthermore the diffusive transport is slow due to the viscosity of the solvent, the underlying differential equations become too stiff to solve them with standard methods in a direct numerical simulation. In such systems in which the time scale of transport processes is much larger than the time scale of the chemical reaction (quasi-instantaneous reaction), the reduction of the set of equations as already introduced in Toor and Chiang[7] is a useful alternative for diffusion-controlled irreversible reactions. For this purpose a new equation is obtained by taking the difference between the transport equations for both reactants. This results in the single transport equation

$$\partial_t \phi + \mathbf{u} \cdot \nabla \phi = \nabla \cdot (D(\phi) \nabla \phi) \tag{7}$$

with

$$\phi = c_{\mathrm{A}} - c_{\mathrm{B}}. \tag{8}$$

Because of the infinite speed and the irreversibility of the reaction, the species A and B cannot coexist. Consequently, $c_{\mathrm{A}} \cdot c_{\mathrm{B}} = 0$ and, hence, at every point one of them is always zero. Thus solving the equation for ϕ eventually yields c_{A} and c_{B} by means of the relations

$$c_{\mathrm{A}} = \max\{\phi, 0\} \quad \text{and} \quad c_{\mathrm{B}} = \max\{-\phi, 0\}. \tag{9}$$

The elimination of the reaction term as explained above yields a pure transport problem which, by means of adapted grids and parallel computing, can be solved numerically under resolution of all involved length scales. Note that different diffusivities for the involved species are allowed because the diffusion coefficient in Eq. 7 may depend on the transported scalar ϕ. Let us note in passing that the model reduction explained above can be verified by means of rigorous mathematical arguments. Here, let us just mention that integrating of Eq. 3 or 4 over the domain V where the chemical reaction occurs, dividing by Da_{I} and letting Da_{I} go to infinity (corresponding to $k \to \infty$) yields

$$\int_V c_{\mathrm{A}} c_{\mathrm{B}} dV = 0. \tag{10}$$

Consequently, $c_{\mathrm{A}} \cdot c_{\mathrm{B}} = 0$ as both concentrations are nonnegative. This is the key point in passing from the convection-diffusion-reaction Eqs. 3 and 4 to the pure transport Eq. 7.

Here, this approach to simulate chemically reacting flows with very fast reactions is applied to the neutralization of aqueous solutions of hydrochloric acid and sodium hydroxide. Because of its rate constant of $k = 10^{11}$ L/(mol s) it is possible to treat this reaction as a quasi-instantaneous one. Furthermore, this reaction allows for an experimental investigation since fluorescent tracers are available which are able to detect one of the reactants – the hydroxyle ions or the protons. For experimental validation using micro-LIF techniques, fluorescein has been chosen as a fluorescent indicator for the hydroxyle ions. Incorporation of this dye as an additional species in the simulations permits the direct comparison of the results from a simulation with the experimental data. In fact, as fluorescein will not be homogeneously distributed in the liquid, its concentration has to be accounted for in the numerical simulation.

Introducing fluorescein as a pH indicator, the investigated chemically reacting system does no longer consist of a single reaction, but is a system of several parallel reactions. Still, also in this more complex system, the neutralization reaction between hydrochloric acid and sodium hydroxide can be considered as an irreversible reaction of second order, i.e.

$$\mathrm{H^+ + OH^- \xrightarrow{k} H_2O}.$$

Both ions react with the fluorescent dye, too. The occurring chemical reactions are

$$\mathrm{H^+ + H_2Fl \underset{k_{-1}}{\overset{k_1}{\leftrightarrows}} H_3Fl^+} \quad (K_1 = 10^{-2.2}),$$

$$\mathrm{H_2Fl + OH^- \underset{k_{-2}}{\overset{k_2}{\leftrightarrows}} H_2O + HFl^-} \quad (K_2 = 10^{-4.4}),$$

$$\mathrm{HFl^- + OH^- \underset{k_{-3}}{\overset{k_3}{\leftrightarrows}} H_2O + Fl^{2-}} \quad (K_3 = 10^{-6.5}).$$

The values given in brackets for the equilibrium constants K_{i} are taken from Guyot et al.[17] The reaction between the hydroxyle group and fluorescein is a deprotonation of the fluorescent dye resulting in a measurable fluorescence signal which indicates a high pH-value due to a local excess of $\mathrm{OH^-}$. The experimental measurements have been performed in Hoffmann et al.[18] by injecting an aqueous mixture of fluorescein with HCl in one of the inlets of the T-microreactor. The alkaline solution has been given into the micro-reactor via the other inlet. For this system, the balance equations for the involved chemical species read as

$$\partial_t c_{\mathrm{H^+}} + \nabla \cdot \mathbf{j}_{\mathrm{H^+}} = -k c_{\mathrm{H^+}} c_{\mathrm{OH^-}} - r_1 \tag{11}$$

$$\partial_t c_{\mathrm{OH^-}} + \nabla \cdot \mathbf{j}_{\mathrm{OH^-}} = -k c_{\mathrm{H^+}} c_{\mathrm{OH^-}} - r_2 - r_3 \tag{12}$$

$$\partial_t c_{\mathrm{H_3Fl^+}} + \nabla \cdot \mathbf{j}_{\mathrm{H_3Fl^+}} = r_1 \tag{13}$$

$$\partial_t c_{\mathrm{H_2Fl}} + \nabla \cdot \mathbf{j}_{\mathrm{H_2Fl}} = -r_1 - r_2 \tag{14}$$

$$\partial_t c_{\mathrm{HFl^-}} + \nabla \cdot \mathbf{j}_{\mathrm{HFl^-}} = r_2 - r_3 \tag{15}$$

$$\partial_t c_{\mathrm{Fl^{2-}}} + \nabla \cdot \mathbf{j}_{\mathrm{Fl^{2-}}} = r_3 \tag{16}$$

with the fluxes

$$\mathbf{j}_i = \mathbf{u} c_i - D_i \nabla c_i \tag{17}$$

and the reaction rates

$$r_1 = k_1 c_{\mathrm{H^+}} c_{\mathrm{H_2Fl}} - k_{-1} c_{\mathrm{H_3Fl^+}}, \tag{18}$$

$$r_2 = k_2 c_{H_2Fl} c_{OH^-} - k_{-2} c_{HFl^-}, \tag{19}$$

$$r_3 = k_3 c_{HFl^-} c_{OH^-} - k_{-3} c_{Fl^{2-}}. \tag{20}$$

Here, k is the rate constant of the neutralization reaction, k_i and k_{-i} are the rate constants of the forward and backward steps of the reversible reactions, and D_i denotes the diffusion coefficient of the i-th component. Diffusion coefficients were taken from Newman.[19] In the rate functions in Eqs. 18 and 19 the species water was neglected as a reactant since it is the solvent and, hence, present in large excess.

Since the concentration of the fluorescent dye is about 1000 times smaller than the concentration of acid and base in the experiments, the source term corresponding to the fluorescein reactions can be neglected. Under this assumption, Eqs. 11 and 12 are simplified to

$$\partial_t c_{H^+} + \nabla \cdot \mathbf{j}_{H^+} = -k c_{H^+} c_{OH^-}, \tag{21}$$

$$\partial_t c_{OH^-} + \nabla \cdot \mathbf{j}_{OH^-} = -k c_{H^+} c_{OH^-}. \tag{22}$$

Guyot et al.[17] found that the neutral as well as the two deprotonated forms of fluorescein show fluorescence where the highest quantum yield of $\eta = 0.92$ is provided by the doubly charged ion Fl^{2-}. The quantum yield of HFl^- is significantly smaller with $\eta = 0.26$, respectively $\eta = 0.14$ for the uncharged form. Münsterer and Jähne[20] considered only the first and second deprotonated forms when they set up the relation between the extinction and the concentrations of fluorescein as

$$M \propto \eta_{HFl^-} \varepsilon_{HFl^-} c_{HFl^-} + \eta_{Fl^{2-}} \varepsilon_{Fl^{2-}} c_{Fl^{2-}}. \tag{23}$$

This relation is suitable within the pH range from pH = 4 to pH = 8 in which they performed their experiments. In the present case, experiments and simulations have been performed within a pH range from pH = 1 to pH = 13 and, hence, all forms of fluorescein can occur. Several forms of fluorescein contribute to the measured fluorescence signal and the contribution of each individual form depends on the local pH value. Unfortunately, it is impossible here to distinguish the individual fluorescent contributions in the measurement of the fluorescent signal. To overcome this problem, we sum up the local concentrations of all forms of fluorescein. This leads to the total concentration of fluorescein, c_{Fl}, given as

$$c_{Fl} = c_{H_2Fl} + c_{H_3Fl^+} + c_{HFl^-} + c_{Fl^{2-}}. \tag{24}$$

Now, because the protonation and deprotonation of fluorescein are very fast chemical reactions, we may assume local equilibrium of the different forms of fluorescein, where the equilibrium concentrations of course depend on the local pH value. On the basis of the given equilibrium constants and the mass action law for each reaction, the local composition regarding the different forms of fluorescein can be calculated from the overall concentration c_{Fl}. Then the local intensity of the fluorescent signal is given by

$$I = a\left(\eta_{H_2Fl} \frac{K_3 K_2}{10^{2(pH-14)}} + \eta_{HFl^-} \frac{K_3}{10^{pH-14}} + \eta_{Fl^{2-}}\right) c_{Fl}, \tag{25}$$

$$a = 1 + \frac{10^{-pH} K_3 K_2}{10^{2(pH-14)} K_1} + \frac{K_3 K_2}{10^{2(pH-14)}} + \frac{K_3}{10^{(pH-14)}}. \tag{26}$$

Summation of Eqs. 13–16 leads to a single transport equation for the total fluorescein concentration, given as

$$\partial_t c_{Fl} + \nabla \cdot \mathbf{j}_{Fl} = 0. \tag{27}$$

Note that no reaction term appears in Eq. 27 because the sum of all partial reactions of fluorescein is zero. In our numerical simulations we then assume that the molecular flux of the total amount of fluorescein can be well approximated by Fick's law with an effective diffusivity. For the latter, the value of 3.67×10^{-10} m^2/s has been chosen which is taken from Münsterer and Jähne.[20]

Having performed these model reductions, it is now possible to follow the approach outlined above. For this purpose we define the quantity ϕ as

$$\phi = c_{OH^-} - c_{H^+} \tag{28}$$

in order to model the neutralization of the acid and the base. Since the concentrations of the reactants are normalized by the inlet concentrations, the values of ϕ lie within the interval $[-1, 1]$, where $\phi < 0$ represents the local existence of H^+, respectively $\phi > 0$ the occurrence of OH^-. By taking the difference of Eq. 20 and, Eq. 21 we obtain Eq. 7 for ϕ. The diffusivities of the leach and the acid are not equal ($Sc = 300$ for the pair H^+/Cl^- and $Sc = 470$ for Na^+/OH^-), hence the diffusion coefficient for the scalar ϕ depends on the value of ϕ according to

$$D(\phi) = \begin{cases} D_{NaOH} & \text{for } \phi \geq 0, \\ D_{HCl} & \text{for } \phi < 0. \end{cases} \tag{29}$$

While the approach given above is well suited for computing the reactive mixing of two reactants in an instantaneous reaction, it will not give the product concentration. Furthermore, local mass conservation of the reaction cannot be used to calculate the local product distribution directly from the current values of the reactant concentrations due to diffusive and convective transport processes. Consequently, since the local product concentration needs to be known in case of consecutive reactions, it remains to solve the stationary reaction-convection-diffusion Eq. 5. But in Eq. 5 the stiff reactive source term appears which has elsewhere been eliminated in the current approach. Note that the kinetic term is localized at a small layer around the interface between the reactants; it is even only active *on* this interface in case of an instantaneous reaction. To circumvent this problem, we use one of the reactant transport equations in order to replace the kinetic term by the net transport of this reactants. Under stationary conditions, the concentration field of the product is therefore determined from

$$\mathbf{u} \cdot \nabla c_P - \frac{1}{Re\, Sc_P} \Delta c_p = \frac{1}{Re\, Sc_A} \Delta c_A - \mathbf{u} \cdot \nabla c_A, \tag{30}$$

where the concentration c_A of species A is obtained from the scalar variable ϕ by means of Eq. 8. The right-hand side of Eq. 30 is calculated for each cell that contains a part of the reaction front (corresponding to a sign change of ϕ) and implemented as a source term. To ensure a complete resolution of all involved length scales, we execute our simulations on an adaptively refined grid, where all those cells in which high gradients of ϕ are found are several times refined. The numerical simulations are performed with FLUENT® (Ansys, USA). Since this CFD-solver cannot handle hanging nodes for the calculation of the right-hand side in[30] inside user-define routines, we were only able to use this approach for the computation of product concentrations on uniform grids, where we employed Finite Differences to calculate the gradients in.[30]

Numerical Setup

The numerical calculations were carried out for a T-shaped micromixer with rectangular cross sections. The geometry is based on a silicon etched channel as shown in Figure 1 (right). The entire mixing channel has a length of 14 mm, both inlet channels have a length of 8 mm. The channel depth and width vary between different T-micromixers used in these investigations. In the default configuration, all parts of the channel have a depth of 100 μm. The width of each inlet channel is 100 μm and that of the mixing channel is 200 μm. For the computational domain, the inlet channels are shortened to have a length of 300 μm. Preliminary calculations have also shown that a reduced length of 1500 μm for the mixing channel is sufficient to avoid back effects of the outlet boundary conditions on the flow inside the mixing zone. A correspondingly reduced domain as shown in Figure 1 (left) is used in the numerical simulations. This allows for a further enhancement of the grid resolution, where the 3D grid consists of cubic cells. This computational domain contains in particular the complete mixing zone of the T-shaped microreactor, where efficient mixing occurs by convection in cross-sectional directions. This mixing zone extends up to about 500 μm into the main channel for the standard mixer geometry (i.e., with 100×200 μm^2 mixing channel).

A fully developed Poiseuille-type velocity profile for flow in a channel of rectangular cross-section is used as a Dirichlet boundary condition for both inlets,[14] combined with a pressure boundary condition at the outlet. At fixed walls we use the no-slip boundary condition. Using these boundary conditions, the Navier-Stokes equations are solved without any additional model or assumption for an incompressible Newtonian solvent to obtain the velocity field which provides the basis for convective species transport.

The numerical simulations were carried out with the commercial CFD-software FLUENT 6.2 which numerically solves the incompressible Navier-Stokes equations together with additional scalar transport equations. The discretisation employs the Finite Volume Method for a block-structured grid composed of about 9 million cubic cells. To account for species which undergo chemical reactions of finite speed, a scalar transport equation with appropriate source term is solved for each such reactant. At the inlet a homogeneous distribution of the reactants is prescribed by means of a corresponding inhomogeneous Dirichlet boundary condition. At fixed walls as well as at the outlet, a homogeneous Neumann boundary condition is applied. Quasi-instantaneous irreversible chemical reactions are included using the approach described in the "*Mathematical Model*" section above. This amounts to solve the transport Eq. 7 with state-dependent diffusivity. For this purpose, the current local diffusivity according to the sign of the variable ϕ is assigned to each computational cell prior to the diffusive transport step. From these cell-specific diffusivities, face-specific diffusion coefficients are computed using harmonic means; cf. Patankar.[21] Let us note in passing that Eq. 7 can be written as the nonlinear diffusion equation, also called filtration equation,

$$\partial_t \phi - \Delta F(\phi) + \mathbf{u} \cdot \nabla \phi = 0, \tag{31}$$

where, F satisfies $F'(r) = D(r)$. While the gradient of ϕ will have a jump at the reaction front where $\phi = 0$, the flux given as $-\nabla F(\phi)$ is continuous there in the generic case; see Vazques[22] for more information on the filtration equation and Tonegawa[23] concerning regularity results for systems with state-dependent diffusivity. Therefore the numerical solution of Eq. 7 or Eq. 31 can be done with standard Finite Volume techniques as explained above. The proof of principle, showing that the combination of Eq. 7 with Eq. 30 enables the computation of both the distribution of reactants and of the product has been provided[24] for a single quasi-instantaneous reaction of type

$$A + B \overset{k \to \infty}{\longrightarrow} P.$$

Figure 2 presents the resulting profiles on a cross section of the microchannel in the complex but stationary engulfment flow; the latter is illustrated by the streamlines shown in Figure 3 below. In the left part of Figure 2 the distribution of the scalar ϕ on a cross-section inside the mixing zone is shown. In this computation, the inlet concentrations were normalized to dimensionless values of $+0.5$ and -0.5, respectively. The plot clearly displays large still unmixed regions of pure reactants, separated by the reaction front where ϕ takes the value zero. The right part of Figure 2 shows the product distribution on the same cross-section. As to be expected, the product is only present close to the reaction front. The different values along this front are explained by different speeds of the fluid particles at different locations. Hence there is locally a different time available for the chemical reaction up to this point is the channel.

In our subsequently described numerical simulations of the full chemical system from the "*Mathematical Model*" section above, the computation of the product distribution is omitted because the generated product water cannot be measured since water, being the solvent, already is the main component.

Results

Due to usually short residence times in microreactors, mixing has to be fast in order to enlarge the contact area between chemically reacting species. While turbulent flow provides fast convective mixing, it requires high energy input resulting in large pressure drops especially for microsystems. Laminar velocity fields with secondary flow exhibit lower pressure drops but can still significantly promote convective mixing. In addition, such flows provide defined flow

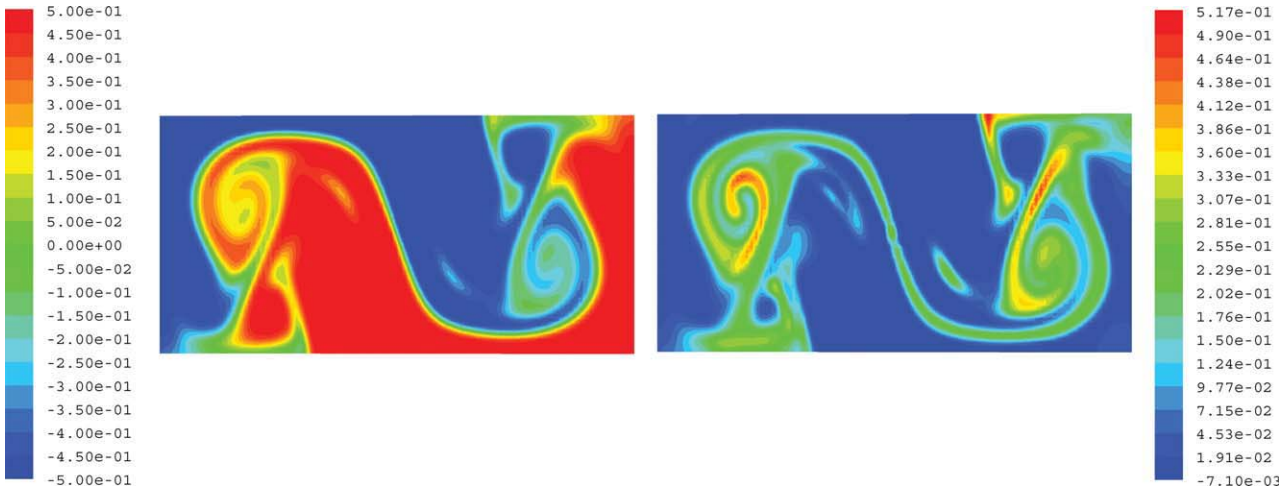

Figure 2. Distribution of the scalar variable Φ (right) and of the product from a neutralization (left) on a cross-section at the beginning of the mixing zone (z = 250 μm, Re = 186).

[Color figure can be viewed in the online issue, which is available at www.interscience.wiley.com.]

conditions. Therefore stationary laminar flows with secondary flow patterns are important for applications in microreactors. For the specific reactor geometry considered here (cf. Figure 1, left), three different stationary flow regimes can be observed up to a Reynolds number of about 240 at which time-periodic flow phenomena set in.[14,16] At Reynolds numbers below 40, strictly laminar flow behavior occurs without secondary flow. Then, for $40 < Re < 138$, the so-called vortex flow regime exhibits secondary flow in form of a double vortex pair. These vortex pairs are formed due to centrifugal forces because the inlet streams turn around the corners from the respective inlet into the mixing channel. The mechanism behind is a centrifugal instability as known from the occurrence of so-called Dean-vortices for flow through a bend. The symmetry with respect to the symmetry plane perpendicular to the inlet channels is destroyed if the Reynolds number exceeds $Re = 138$. In this case fluid elements reach the opposite side of the mixing channel, as illustrated by the streamlines displayed in Figure 3, resulting in good cross-directional mixing. Consequently, among these stationary laminar flow conditions the engulfment flow is the most effective one and leads to a rapid increase of the contact area between the two inlet flows. For more information on the obtained quality of mixing and scale of segregation in this T-microreactor see Bothe et al.[15]

Using the numerical approach described above, the numerical simulation of a neutralization reaction between hydrochloric acid and sodium hydroxide has been performed on a Cartesian grid of 9 million cubic grid cells. The local fluorescent signal intensity at the local pH-value is computed in each cell by using Eq. 24. For the computation of the chemical reaction, the acid/base system (represented by the passive scalar ϕ from Eq. 7 and the fluorescent dye are injected into the opposite inlet channels.

The concentration distribution of the fluorescence dye from our simulations has been qualitatively compared with experimental data of our cooperation partner at the IUV Bremen (Prof. Räbiger, Dr. Schlüter). For this purpose, a microreactor with an aspect ratio of 0.45 with a channel width of 600 μm and a height of 270 μm is used both in the experiments and in the simulations. Since the measurements are carried out with confocal microscopy, which collects the fluorescence signal from a given measurement volume of fixed size, the enlarged dimensions have the advantage of a higher relative resolution (i.e., a larger number of pixels per channel cross section) in the experimental measurements. The Reynolds-number for which the experimental data has been measured is $Re = 250$. Figure 4 (bottom) shows the experimentally obtained fluorescent signal intensity on a cross section at 250 μm down the mixing channel (cf. Hoffmann et al. [18]). The measurement corresponds to a Reynolds number of 250 and the above mentioned channel geometry.

In the same figure (Figure 4, top) the result of the numerically obtained species distribution is displayed. In the numerical simulations the grid is adaptively refined in several steps during the calculation to obtain a sufficiently high resolution in those regions where steep gradients of the scalar ϕ occur. This way the scalar quantities were resolved with local cell size of about 2 μm near the reaction front for cross-sectional channel dimensions of 600 $\times$ 270 μm. The result of this simulation is grid independent in the sense that a further local refinement does not reveal additional structures in the solution. As mentioned above, the distribution of

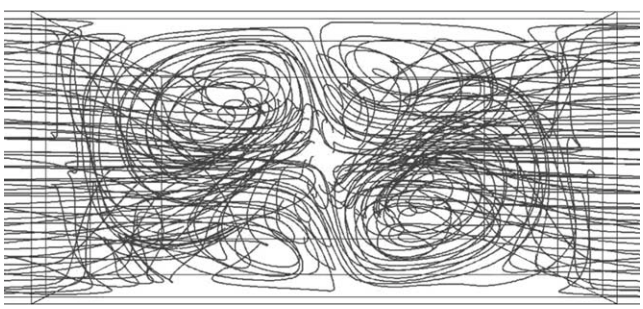

Figure 3. Streamlines at the beginning of the mixing zone (Re = 149).

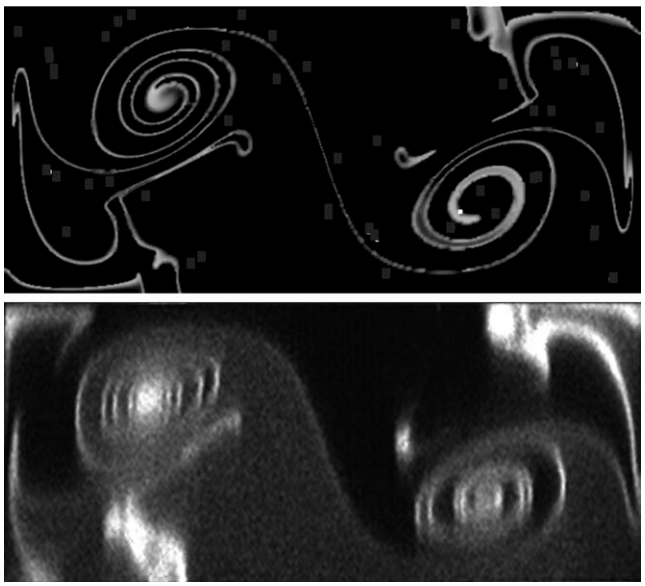

Figure 4. Numerically (top) and experimentally (bottom) obtained signal intensity of the fluorescence tracer on a cross section at 250 μm down the mixing channel.

two passive scalars with different diffusivities is computed in order to capture the system of chemical reactions. Here, one scalar represents the distribution of both HCl and NaOH, while the other one represents the distribution of fluorescein. The resulting signal intensity is determined by Eq. 25. The comparison between experiment and simulation shows a very good overall accordance. It can also be seen that even small isolated structures are captured in the numerical computation.

For a mean velocity of 2.0 m/s ($Re = 250$), Figure 5 shows the pH-distribution (left), the distribution of the dye (middle) and the corresponding fluorescence signal intensity (right) on a cross section on half of the height of the mixing channel. The fluorescence signal occurs only in those regions, where both the fluorescence dye (fluorescein) and a high pH-value are present. Due to the fact that the two scalars have different Schmidt numbers (diffusivities) of 300 and 470 for HCl and NaOH, respectively, and approximately 3600 for the dye, small differences in their distributions occur. These small differences lead to the highly asymmetric fluorescence signal in Figure 5 (right).

In further simulations with the standard geometry as describes above, the signal intensities of the dye are obtained for a mean velocity of 0.9 m/s ($Re = 120$) and 1.2 m/s ($Re = 160$). In addition to the signal intensities, the conversion of the neutralization reaction is evaluated on single cross sections along the mixing channel. Furthermore, the specific contact area between the acid and the base is evaluated on each of the investigated cross sections. The specific contact area is obtained by means of the expression[14]

$$\frac{1}{|V|}\int \| \nabla f \| \, dV \quad \text{with} \quad f = \phi/\phi_{\max}. \tag{32}$$

In Eq. 32 the integrand is the Euclidean norm of the gradient of the normalized scalar. In the present case of a segregated system in which f changes from -1 to $+1$ across a small layer around the reaction front, the quantity in[32] is an excellent approximation of twice the area of the front per total volume. Here, the computations are done for cross

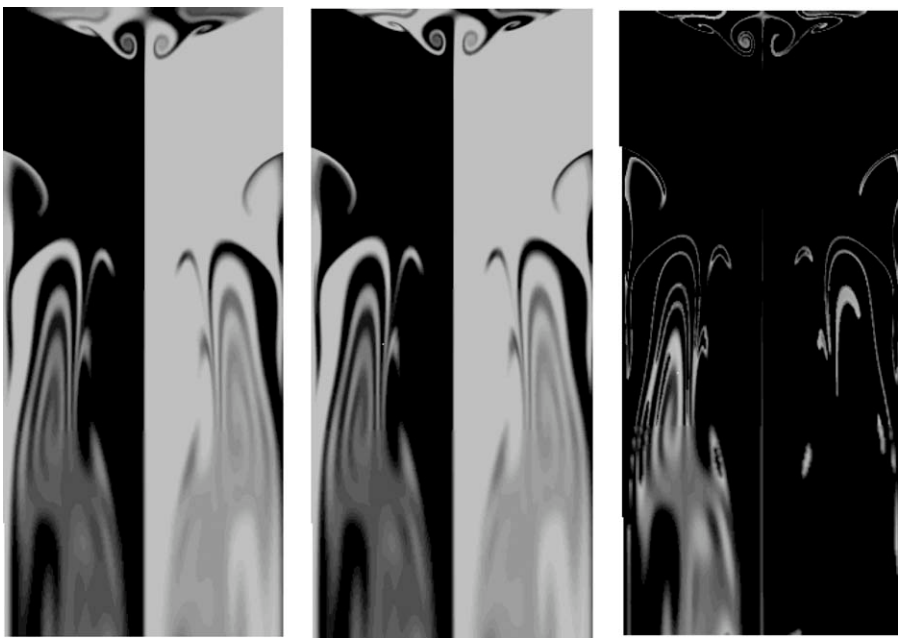

Figure 5. Simulated quantities on the cross-section at half of the height of the mixing channel.

pH-value distribution (left) in the range of pH 3 (black) and pH 11 (white), the distribution of fluorescent (middle) and the signal intensity (right). $Re = 250$, mixing channel aspect ratio = 0.45.

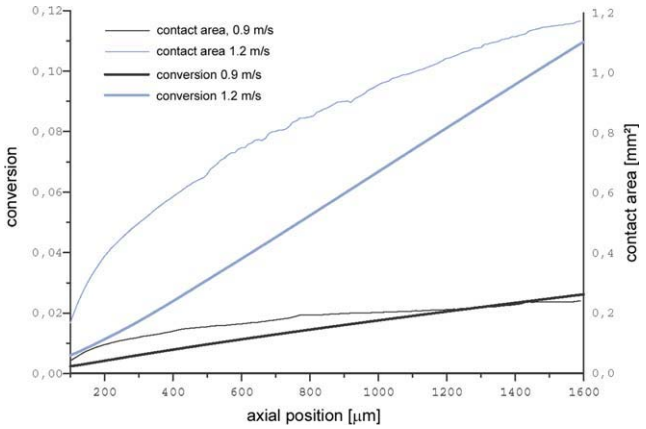

Figure 6. Conversion and contact area along the mixing channel for different mean velocities.

[Color figure can be viewed in the online issue, which is available at www.interscience.wiley.com.]

sections in which case Eq. 32 yields the specific length of the line of the reaction front.

Figure 6 displays the achieved conversion as well as the contact area for two different laminar flow regimes. The contact area is the region in which the reactants of the quasi-instantaneous reaction meet each other and, hence, where the product is formed. It can be seen that slow generation of contact area in case of small Reynolds numbers leads to a weak conversion. In contrast, high Reynolds numbers lead to enhanced conversion.

Scaling Effects

For given geometrical similarity, the flow behavior is solely determined by the Reynolds number regardless of the dimensions of the device, if the in- and outlet conditions are scaled correspondingly. For the complete system of model Eqs. 1 and 2, hydrodynamical *and* physico-chemical similarity cannot be achieved simultaneously for reactors of different size. Note that for fixed ratio d/L not both numbers—the Reynolds number and the Damköhler number - can be kept fixed while changing the size:

$$Re' = Re, \qquad Sc' = Sc, \quad \text{but} \quad Da_{\mathrm{I}}' = \lambda^2 Da_{\mathrm{I}}. \tag{33}$$

If all lengths are changed by a factor $\lambda << 1$ while Re is kept fixed, then $L' = \lambda\ L$, $d_h' = \lambda\ d_h$ and $U' = U/\lambda$. The resulting dimensionless species equations read as

$$\partial_t c_i + \mathbf{u} \cdot \nabla c_i = \frac{1}{Re\ Sc_{\mathrm{i}}} \Delta c_i + \lambda^2 \frac{d_h}{L} Da_{\mathrm{I}} c_i^n. \tag{34}$$

Scaling down the reactor dimensions significantly reduces the characteristic times of the transport processes relative to the (fixed) time scale of the chemical reaction. Hence, in particular, quasi-instantaneous chemistry is maximally affected by transport limitations. Therefore the change of the reactor dimensions leads to a shift in the range of accessible reaction times, i.e. certain reactions that are too fast to be performed in a macro-scale reactor can be accomplished in micro-scale systems.

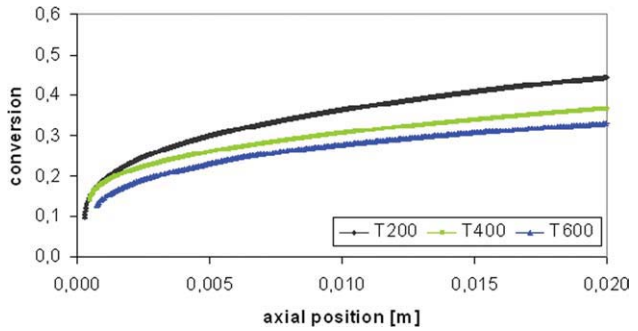

Figure 7. Conversion of reactants in the neutralization reaction, Re = 186.

[Color figure can be viewed in the online issue, which is available at www.interscience.wiley.com.]

To investigate such scale effects on the interplay between transport processes and chemical reactions, three geometrically similar T-microreactors have been studied in the engulfment flow regime at $Re = 186$. The smallest one is denoted T-200 with dimensions of 200 μm for the width, 100 μm for the high and 20 mm for the length of the microchannel. In addition, two scaled versions of this microreactor, abbreviated as T-400 and T-600, are used the dimensions of which are two, respectively three times larger. The studied chemical reaction is an irreversible and instantaneous reaction between reactants A and B to form one or more products. As expected from the general considerations above, it turns out that also in a microreactor this reaction is still limited by the transport processes. Due to the small diffusion time, the T-200 microreactor provides the highest conversion as can be seen in Figure 7. Here the conversion C_{A} of reactant A at an axial position z is defined as

$$C_{\mathrm{A}} = 1 - \dot{n}_{\mathrm{A}}^{\mathrm{out}}(z)/\dot{n}_{\mathrm{A}}^{\mathrm{in}} \tag{35}$$

with $\dot{n}_{\mathrm{A}}^{\mathrm{out}}(z)$ being the flux of reactant A in outflow direction through the cross section at a given axial position z.

If the scaling behavior of the dimensions is taken into account, i.e. if the conversion is plotted against a rescaled axial position as shown in Figure 8, it turns out that all three reactors provide the same conversion. This is reasonable since the reaction is limited by the diffusive transport and

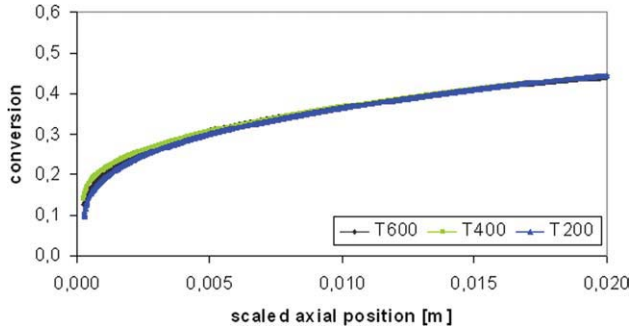

Figure 8. Conversion of reactants taking scaled axial position into account, Re = 186.

[Color figure can be viewed in the online issue, which is available at www.interscience.wiley.com.]

this is especially true for an instantaneous chemical reaction. Indeed, in the limiting case of an instantaneous reaction, the conversion is completely determined by the solution of Eqs. 2 and 7. Now Eq. 7 shows the same invariance under rescaling of the dimensions as Eq.1 without chemical reaction. Therefore the conversion as a function of the scaled axial coordinate is not influenced by the reactor dimensions if the channel geometry as well as the Reynolds and Schmidt number are kept constant. Transforming the solutions back into the original dimensional system, this implies an increase of the space-time-yield proportional to λ^{-2}. To see the latter, recall that for a continuous process the space-time-yield is defined as the rate at which product leaves the reactor by the reactor volume. In our case this is given by

$$\frac{1}{|V|}\int_{A^{out}} c_P \mathbf{u}\cdot\mathbf{n}dA, \tag{36}$$

where, P denotes the product. From the above line of arguments it follows that c_P stays constant, while $\mathbf{u}$ scales with λ^{-1}. Together with the obvious scaling of area and volume, the stated proportionality follows.

Conclusions

The employed method approximates the reactive liquid mixing with convection, diffusion and fast irreversible reaction by means of passage to a quasi-instantaneous, i.e., infinitely fast reaction which can then be eliminated from the system. This approach is well-suited for realistic fully 3D numerical simulations as shown by comparison with existing experimental data for the neutralization of hydrochloric acid and sodium hydroxide performed in a T-microreactor. Using this chemical reaction as an example we are able to show that down-scaling of the reactor dimensions leads to significantly enhanced conversion and space-time-yield. The observed scaling effect underlines the potential of microreactors to intensify processes with fast reactions.

An important additional feature of our approach is the possible computation of the generated product concentration. This is obtained from mass flux calculations where the reactive source term is again eliminated. Hence the overall approach allows for the computational analysis of more complex reaction systems in which the product of a fast irreversible reaction undergoes consecutive chemical transformations. This enables investigations of the performance of, e.g., microreactors for chemical engineering purposes in the case of fast chemistry. These fast reactions are limited by transport processes, an effect which is especially strong if the reactions are performed in macro-systems. Using the limiting case of quasi-instantaneous reactions, numerical simulations will help to identify measures which are most effective to reduce the transport limitations.

Acknowledgments

The authors gratefully acknowledge financial support from the German Research Foundation (DFG) within the priority program 1141 "Analysis, Modeling and Calculation of Mixing Processes with and without Chemical Reactions". We also thank the Paderborn Center for Parallel Computing (PC^2) for technical support and provided computation time.

Notation

c = molar concentration
C = conversion
D = diffusion coefficient
d = diameter
K = equilibrium constant
k = rate constant
I = intensity
L = length of the microchannel
M = extinction
n = order of the reaction
$\dot{n}$ = molar flux
p = pressure
r = rate of a chemical reaction
t = time
U = mean velocity
z = axial coordinate
$\mathbf{u}$ = velocity vector
$\mathbf{j}$ = flux vector
Da_I = Damköhler number
Re = Reynolds number
Sc = Schmidt number
ε = extinction coefficient
ϕ = scalar
λ = scaling factor
η = quantum yield
ν = kinematic viscosity

Subscripts

i = species number
h = Hydraulic

Literature Cited

1. Baldyga J, Bourne JR. *Turbulent mixing and chemical reactions*. New York: John Wiley & Sons, 1999.
2. Fox RO. *Computational models for turbulent reacting flows*. Cambridge: Cambridge University Press, 2003.
3. Troelstra EJ, van Lune J, van Dierendonck LL, Janssen LPBM, Renken A. Modeling of a Buss-Kneader as a polymerization reactor for acrylates. Part I: model validation. *Polym Eng Sci*. 2002;42:230.
4. Linjie Z, Narh KA, Hyun KS. Investigation of mixing mechanisms and energy balance in reactive extrusion using three-dimensional numerical simulation method. *Int J Heat Mass Transfer*. 2005;48:3411–3422.
5. Hessel V, Hardt S, Löwe H. *Chemical micro process engineering*. Weinheim: Wiley-VCH, 2004.
6. Szalai ES, Kuhura J, Arratia PE, Muzzio FJ. Effect of hydrodynamics on reactive mixing in laminar flow. *AIChE J*. 2003;49:168–179.
7. Toor H, Chiang S. Diffusion-controlled chemical Reactors. *AIChE J*. 1959;5:339–344.
8. Muzzio FJ, Ottino JM. Dynamics of a lamellar system with diffusion and reaction: scaling analysis and global kinetics. *Phys Rev A*. 1989;40:7182–7192.
9. Muzzio FJ, Ottino JM. Evolution of a lamellar system with diffusion and reaction: a scaling approach. *Phys Rev Lett*. 1989;63:47–50.
10. Sokolov IM, Blumen A. Mixing effects in the A+B→0 reaction-diffusion scheme. *Phys Rev Lett*. 1991;66:1942–1945.
11. Sokolov IM, Blumen A. Mixing diffusion-controlled reactions in lamellar systems. *Phys Rev A*. 1991;43:2714–2719.
12. Cerbelli S, Garofalo F, Giona M. Steady-state performance of an infinitely fast reaction in a three-dimensional open Stokes flow. *Chem Eng Sci*. 2008;63:4396–4411.
13. Stemich C. Theoretische und numerische Untersuchung des Strömungsmischens in einem T-förmigen Mikromischer. Ph.D. thesis, University of Paderborn, 2006.
14. Bothe D, Stemich C, Warnecke HJ. Fluid mixing in a T-shaped micro-mixer. *Chem Eng Sci*. 2006;61:2950–2958.

15. Bothe D, Stemich C, Warnecke HJ. Computation of scales and quality of mixing in a T-shaped microreactor. *Comp Chem Eng*. 2008; 32:108–114.
16. Dreher S, Kockmann N, Woias P. Characterization of Laminar Transient Flow Regimes and Mixing in T-shaped Micromixers. *Heat Transfer Eng*. 2009;30:91–100.
17. Guyot G, Arnaud R, Lemaire J. Emission des différentes formes de la fluorescéine en solution aqueuse. *J Chem Phys*. 1975;72: 647–653.
18. Hoffmann M, Schlüter M, Räbiger N. Experimental investigation of liquid–liquid mixing in T-shaped micro-mixers using μ-LIF and μ-PIV. *Chem Eng Sci*. 2006;61:2968–2976.
19. Newman JS. *Electrochemical systems*, 2nd ed. Englewood Cliffs, N.J.: Prentice-Hall Inc., 1991.
20. Münsterer T, Jähne B. LIF measurements of concentration profiles in the aqueous mass boundary layer. *Exp Fluids*. 1989;25:190–196.
21. Patankar SV. *Numerical heat transfer and fluid flow*. Washington, DC: Hemisphere, 1980.
22. Vázquez JL. *The porous medium equation, mathematical theory*. Oxford: Clarendon Press, 2007.
23. Tonegawa Y. On the regularity of a chemical reaction interface. *Commun Partial Diff Eqs*. 1998;23:1181–1207.
24. Bothe D, Lojewski A, Warnecke HJ. Direct numerical simulation of reactive mixing in a T-shaped micro-reactor. In: FEDSM2007–37507 (Extended Abstract) in Proceedings 5th Joint ASME / JSME Fluids Engineering Conference, San Diego, CA, 2007.

Manuscript received Mar. 13, 2009, and revision received Aug. 4, 2009.